Photocatalytic Activity for Water Decomposition of Indates with Octahedrally Coordinated d^{10} Configuration. II. Roles of Geometric and Electronic Structures

J. Sato,[†] H. Kobayashi,[‡] and Y. Inoue*,[†]

Department of Chemistry, Nagaoka University of Technology, Nagaoka 940-2188, Japan, and Department of Chemistry and Bioscience, Kurashiki University of Science and The Arts, Kurashiki 712-8505, Japan

Received: January 9, 2003; In Final Form: April 23, 2003

The effects of electronic and local structures on the photocatalytic activities for water decomposition of different kinds of indates [MIn_2O_4 (M = Ca, Sr), $Sr_{0.93}Ba_{0.07}In_2O_4$, and $AInO_2$ (A = Li, Na)] were studied. Raman spectroscopic measurements were performed to characterize their structures. The geometric structures of InO_6 octahedral units were compared among the indates, and it was shown that the photocatalytically active indates possessed distorted InO_6 octahedra with dipole moment, and there was a correlation between the photocatalytic activities and the dipole moment. A plane-wave density function theory (DFT) was applied to calculate the density of state and band energy diagram for $SrIn_2O_4$. The valence band was composed of the O 2p orbital, whereas the conduction band consisted of the hybridized In 5s5p orbitals with large dispersion, indicative of large mobility of photoexcited electrons in the conduction band. The electronic feature of $SrIn_2O_4$ was compared with that of a representative transition metal oxide of $BaTi_4O_9$ with an octahedrally coordinated d^0 metal ion. On the basis of the electronic and geometric consideration, a mechanism is proposed: internal fields due to the dipole moment promote the charge separation, while the broad sp conduction bands with large dispersion permit photoexcited electrons to move to RuO_2 particles dispersed as a promoter.

Introduction

In a previous paper,[1] the photocatalytic properties of different kinds of the indates such as MIn_2O_4 (M = Ca, Sr), $Sr_{1-x}Ca_xIn_2O_4$ (x = 0.25, 0.5, 0.75), $Sr_{1-x}Ba_xIn_2O_4$ (x = 0.07), and $LnInO_3$ (Ln = La, Nd) have been reported. In the presence of dispersed RuO_2 particles, the photocatalytic activity increased in the order $CaIn_2O_4$ > $SrIn_2O_4$, $Sr_{0.93}Ba_{0.07}In_2O_4 \gg LaInO_3$, $NdInO_3$ under Xe lamp illumination. The activity of $Sr_{1-x}Ca_xIn_2O_4$ increased monotonically with increasing x. In view of photocatalytic differences, it is strongly desirable to correlate them with differences in the electronic states and specific crystal structures of the indates.

Photocatalysis of metal oxides is controlled by three processes. The first is the formation of photoexcited charges by light illumination, the second is charge transfers to the surface without recombination, and the third is the transfer to the reactants adsorbed on the surface. Although it is apparent that the third step is associated with the contribution of promoters (frequently RuO_2 and NiO have been employed) deposited on the metal oxide surfaces, no clear concepts have so far been established with what kinds of factors are useful for the first and second steps. For the better design of photocatalysts for water decomposition, it is important to propose a model for these steps.

The first step is related to the efficiency of photoexcited charge separation, and the second is associated with the prevention of the recombination of photoexcited charges. Our simple assumption is that the geometric structure, for example, an InO_6 octahedron as a fundamental unit, plays an important role in the first step and that the nature of conduction bands is important for the second step. Thus, we have paid attention to the geometric structures of InO_6 octahedron and also to their electronic structures.

To confirm the first assumption, the characteristic photocatalysis of RuO_2-dispersed MIn_2O_4 (M = Ca, Sr) and $Sr_{1-x}Ba_xIn_2O_4$ (x = 0.07) was compared with that of RuO_2-dispersed $LaInO_3$ and $AInO_2$ (A = Li, Na). The activity of the latter was reexamined under Xe lamp irradiation, since the photocatalytic activity of RuO_2-dispersed $AInO_2$ (A = Li, Na) had been investigated only under Hg−Xe lamp illumination.[2] The activity differences were discussed on the basis of the geometric InO_6 octahedral structures, in particular, the extent of InO_6 octahedron distortion which led to the generation of dipole moments. A correlation between the photocatalytic activity and dipole moments was examined.

For the electronic structures, we have calculated the band structures by taking $SrIn_2O_4$ as a representative indate. To see difference and similarity in the band structures between d^{10} and d^0 configurations, the electronic structure of a photocatalytically active transition metal oxide, $BaTi_4O_9$, with d^0 configuration was investigated, because $SrIn_2O_4$ and $BaTi_4O_9$ have similar pentagonal prism tunnel structures,[3−6] as shown in Figure 1. The energy band dispersion diagram and the density of state (DOS) were obtained by the plane-wave-density function theory (DFT) calculation. Based on the geometric and electronic structures, a mechanism of photocatalysis by the indates with octahederally coordinated d^{10} configuration is proposed.

Experimental Section

The photocatalysts of RuO_2-dispersed MIn_2O_4 (M = Ca, Sr), $Sr_{0.93}Ba_{0.07}In_2O_4$, and $AInO_2$ (A = Li, Na) were prepared by the same preparation method as that described in a previous

[†] Nagaoka University of Technology.
[‡] Kurashiki University of Science and The Arts.

10.1021/jp030021q CCC: $25.00
Published on Web 07/12/2003

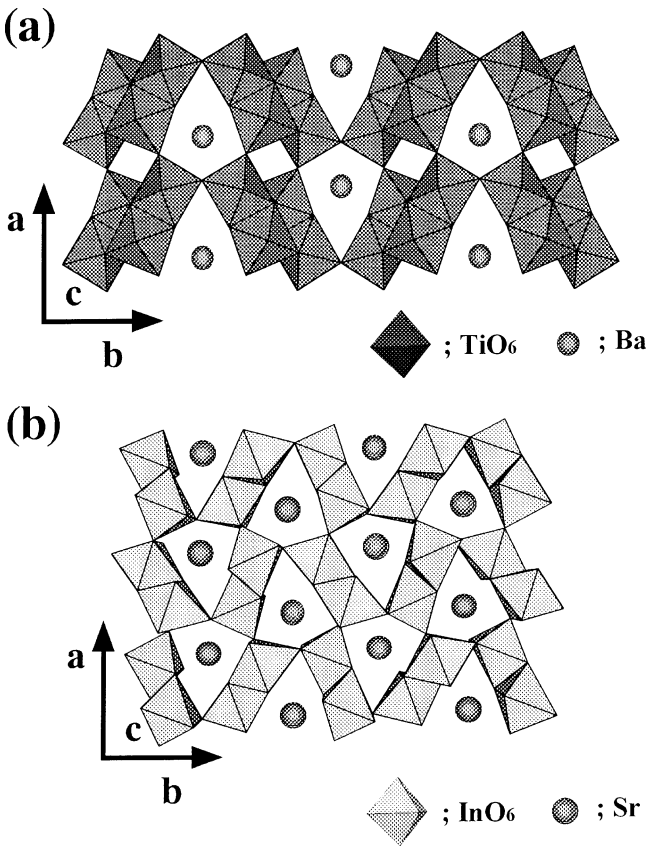

Figure 1. Schematic representations of tunnel structures for $BaTi_4O_9$ (a) and $SrIn_2O_4$ (b).

study.[1,2] The laser Raman spectra were recorded at room temperature on a Jasco 1000 spectrometer.

The plane-wave-based density function theory (DFT) calculation of $SrIn_2O_4$ was performed with the CASTEP program.[7] The core electrons were replaced by the ultrasoft core potentials,[8] and the valence electronic configurations were $4s^24p^65s^2$ for Sr, $4d^{10}5s^25p^1$ for In, and $2s^22p^4$ for O atom. The primitive unit cell consisted of $[SrIn_2O_4]_4$, and the number of occupied orbitals was 120. For $BaTi_4O_9$, the valence electronic configurations were $5s^25p^66s^2$ for Ba, $3s^23p^63d^24s^2$ for Ti, and $2s^22p^4$ for O atom. The unit cell size was $[BaTi_4O_9]_2$, and the number of occupied orbitals was 112. The kinetic energy cutoff was 260 eV for both systems.

Results

Figure 2 shows the photocatalytic activities of RuO_2-dispersed indates under Xe lamp irradiation. RuO_2-dispersed $CaIn_2O_4$ showed the highest activity, whereas $SrIn_2O_4$ and $Sr_{0.93}Ba_{0.07}In_2O_4$ exhibited considerable and similar activities. On the other hand, RuO_2-dispersed $LaInO_3$ produced a small amount of hydrogen only. RuO_2-dispersed $LiInO_2$ and $NaInO_2$ showed negligible photocatalytic activity.

Figure 3 shows the Raman spectrum of $CaIn_2O_4$, $SrIn_2O_4$, $Sr_{0.93}Ba_{0.07}In_2O_4$, and $NaInO_2$. The spectrum of $CaIn_2O_4$ consisted of five major peaks appearing at 200, 262, 328, 406, and 545 cm^{-1} in the wavenumber region 200−600 cm^{-1}. The strongest peak was observed at 545 cm^{-1}, which was assigned to a vibration mode having a symmetry of $\nu_1(A_{1g})$. For $SrIn_2O_4$, a similar spectrum was observed: the peak positions were 191, 236, 321, 395, and 542 cm^{-1}, in which the highest wavenumber of 542 cm^{-1} provided the strongest peak. The Raman spectrum for $Sr_{0.93}Ba_{0.07}In_2O_4$ showed a close similarity to that of

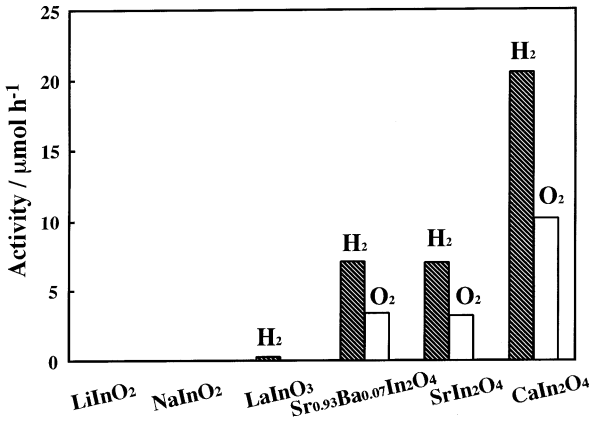

Figure 2. Photocatalytic activities for water decomposition of RuO_2-dispersed indates under Xe lamp irradiation.

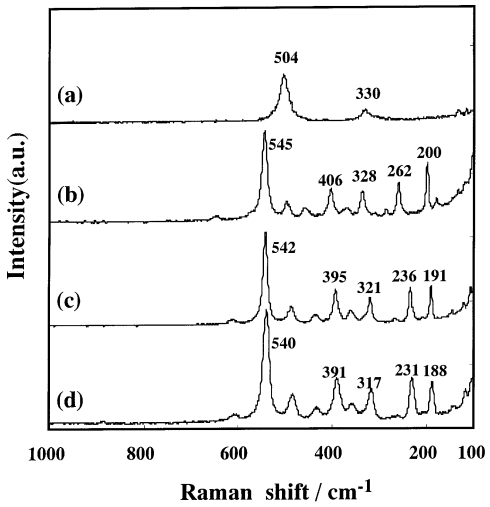

Figure 3. Raman spectra of $NaInO_2$(a), $CaIn_2O_4$(b), $SrIn_2O_4$(c), and $Sr_{0.93}$ $Ba_{0.07}In_2O_4$(d).

$SrIn_2O_4$: the major five peaks were observed at 188, 231, 317, 391, and 540 cm^{-1}, in which the strongest peak appeared at 540 cm^{-1}. On the other hand, $NaInO_2$ showed two peaks at 330 and 504 cm^{-1}.

Figure 4 shows the energy band dispersion diagram and density of states (DOS) for $SrIn_2O_4$. The DOS showed five occupied bands and part of an unoccupied band. The lowest band consisted of the Sr 4s atomic orbital (AO). The second, third, and fourth bands were made up of the O 2s, Sr 4p, and In 4d AOs, respectively. The fifth, i.e., the highest occupied band, corresponded to the broad valence band, which was composed of the O 2p orbital. As for the unoccupied energy levels, the bottom of conduction band was formed by the hybridization of In 5s and 5p AOs, with a small contribution of the O 2p AO, whereas the upper part of the band was associated with the Sr 5s and 4d orbitals. Thus, the highest occupied and lowest unoccupied molecular orbital (HOMO and LUMO) levels were composed of the O 2p orbital and the hybridized In 5s and 5p orbitals, respectively. The band gap was calculated to be 2.09 eV. In the energy band diagram, the valance band was rather flat, and its dispersion was small. By contrast, the conduction band had a large dispersion.

Figure 5 shows the energy band dispersion diagram and DOS for $BaTi_4O_9$. The first band with the lowest energy consisted of the Ti 3s orbital. With increasing energy, the bands corresponding to the Ti 3p, Ba 5s, O 2s, and Ba 5p AOs

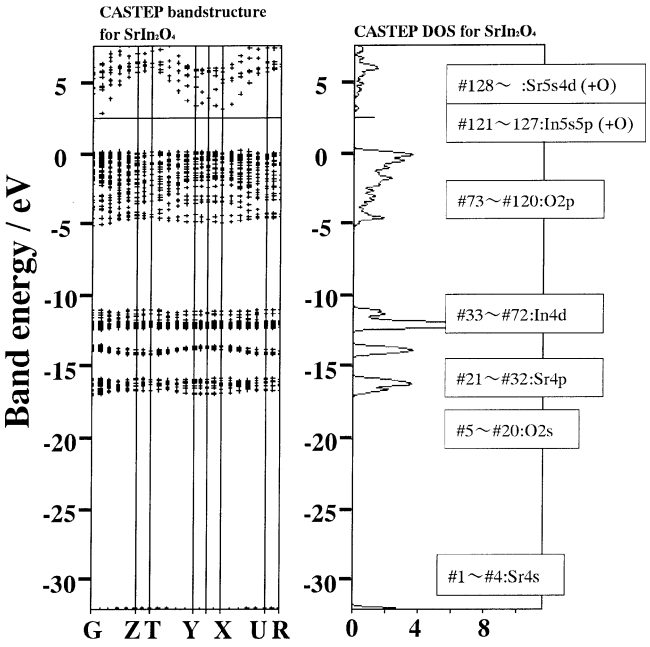

Figure 4. Energy band dispersion diagram and DOS for $SrIn_2O_4$.

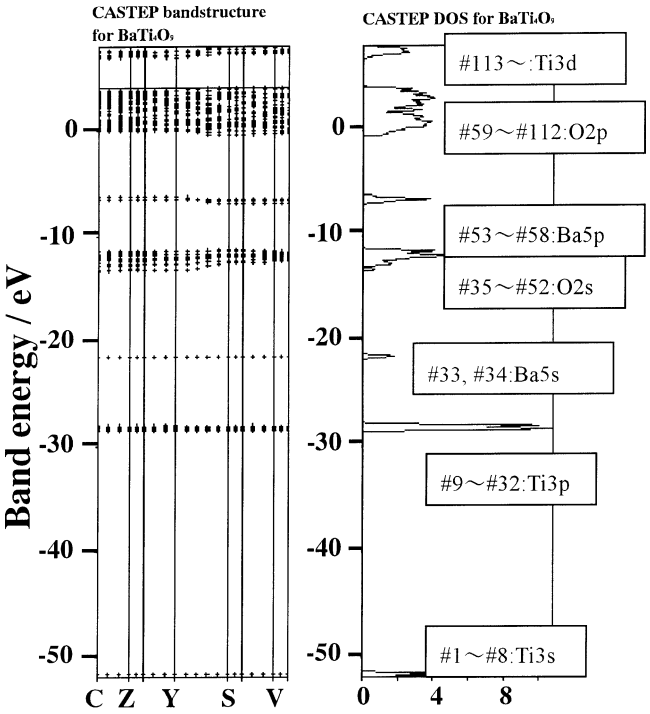

Figure 5. Energy band dispersion diagram and DOS for $BaTi_4O_9$.

appearing in order. The highest-occupied energy band, i.e., the valence band, was formed by the O 2p orbital. The unoccupied conduction band was composed of the Ti 3d orbital. Thus the O 2p and Ti 3d AOs were responsible for the HOMO and LUMO levels, respectively, which was very similar to the electronic structure of TiO_2. The band gap was calculated to be 2.84 eV for $BaTi_4O_9$.

Discussion

$CaIn_2O_4$, $SrIn_2O_4$ and $Sr_{0.93}Ba_{0.07}In_2O_4$ possess an orthorhombic crystal structure: the unit cell of $CaIn_2O_4$ is $a = 0.965$, $b = 1.13$, and $c = 0.321$ nm,[9] and that of $SrIn_2O_4$ is $a = 0.9809$, $b = 1.1449$, and $c = 0.3265$ nm.[3] $Sr_{0.93}Ba_{0.07}In_2O_4$ has a unit

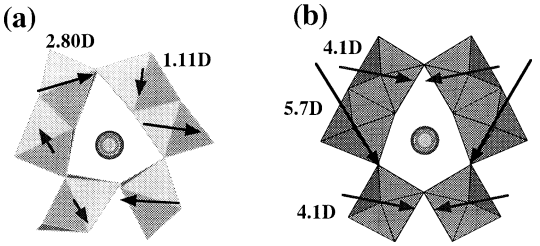

Figure 6. Dipole moments in $SrIn_2O_4$ (a) and $BaTi_4O_9$ (b).

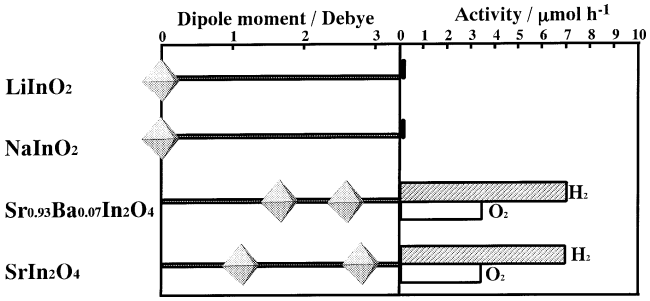

Figure 7. Correlation between photocatalytic activity and dipole moment. The octahedral structures represent InO_6 units.

cell of $a = 0.9858$, $b = 1.152$, and $c = 0.3273$ nm.[10] Their Raman peaks appeared at nearly the same positions, indicating that the these indates have nearly the same crystal structures (Figure 3). The interesting feature is the presence of a pentagonal-prism-like tunnel structure in the three indates. $LaInO_3$ consists of an orthorhombic structure with a unit cell of $a = 1.1402$, $b = 1.1796$, and $c = 0.8198$ nm.[11] $NaInO_2$ has a hexagonal structure with a unit cell of $a = 0.3232$ and $b = 1.639$ nm, $\alpha = \beta = 90°$, and $\gamma = 120°$ [12] and is characterized by the macroscopic morphology of a layer structure. $LiInO_2$ is tetragonal with a unit cell of $a = 0.4312$ and $b = 0.9342$ nm.[13]

The X-ray diffraction data that permit the determination of the local positions of constituent ions are available for $LiInO_2$, $NaInO_2$, $Sr_{0.93}Ba_{0.07}In_2O_4$, and $SrIn_2O_4$ in the references. Using the atom positions, we have calculated the center of gravity of six oxygen ions surrounding an In^{3+} ion. For the four indates, the calculations showed that the InO_6 octahedra were so heavily distorted that the center of the gravity deviated from the position of the In^{3+} ion, generating dipole moments in the octahedral unit. In $SrIn_2O_4$, there were two kinds of the InO_6 octahedral units: one dipole moment was 2.80 D (debyes), and the other 1.11 D, as shown in Figure 6a. For $Sr_{0.93}Ba_{0.07}In_2O_4$, the dipole moments were 1.70 and 2.58 D. On the other hand, $LiInO_2$ and $NaInO_2$ had the normal InO_6 nearly free from distortion, for which the dipole moment was zero. Figure 7 compares photocatalytic activity with dipole moment. The indates with dipole moments are photocatalytically active, whereas the distortion-free indates exhibited negligible activity, indicating that a correlation exists between the photocatalytic activity and the dipole moment. Unfortunately, no crystallographic data regarding the atom positions for $LaInO_3$ and $CaIn_2O_4$ were available. For $CaIn_2O_4$, however, the In−O bond length was reported. $CaIn_2O_4$ has the two kinds of InO_6 octahedra: one octahedron is composed of six In−O bonds with 0.219 (two), 0.218 (two), 0.213, and 0.206 nm, and the other with 0.222, 0.219, 0.218 (two), and 0.209 (two) nm ("two" in parentheses means the presence of the same bond length).[14] The In−O bond lengths were dispersed as broadly as those of $SrIn_2O_4$, suggesting that the InO_6 octahedra are significantly distorted. In addition, the resemblance of Raman peaks to those of $SrIn_2O_4$ indicates the presence of largely distorted InO_6 structures in $CaIn_2O_4$. Thus, it is apparent that a correlation between photocatalytic activity

and dipole moment is true for $CaIn_2O_4$. In a previous study,[15] $M_2Sb_2O_7$ (M = Ca, Sr), $CaSb_2O_6$, and $NaSbO_3$ have been shown to be photocalytically active for water decomposition when combined with RuO_2. These active alkaline earth metal antimonates and sodium antimonate had distorted SbO_6 octahedra. Furthermore, our recent preliminary studies[16] of RuO_2-dispersed MGa_2O_4 (M = Mg, Sr, Ba) photocatalysts showed interesting activity dependence on the kinds of the alkaline earth metal ions, M. The photocatalytic activity was negligible for M = Mg, which had a distortion-free GaO_6 octahedron, whereas the activities were significant for M = Sr and Ba, both of which possessed distorted GaO_4 tetrahedra with dipole moments. Thus, it is evident that the activity dependences on M are strongly associated with the presence and absence of distorted tetrahedral and octahedral units. As previously reported, RuO_2-dispersed $BaTi_4O_9$ and $Na_2Ti_6O_{13}$ showed high photocatalytic activities for water decomposition.[17−20] $BaTi_4O_9$ has two kinds of TiO_6 octahedra, both of which are so heavily distorted that they have dipole moments of 5.7 and 4.1 D[4,5] (Figure 6b). $Na_2Ti_6O_{13}$ has distorted TiO_6 octahedra with dipole moments of 6.7, 5.8, and 5.3 D.[21] Thus, it should be noted that the correlation between the photocatalytic activity and dipole moment is true for both metal oxides with d^{10} and d^0 configuration. The local internal fields due to the dipole moment are considered to be useful for electron−hole separation upon photoexcitation.

The DFT calculations for $SrIn_2O_4$ showed that the valence band consisted of 48 orbitals, which was the number when all the O 2p AOs for 16 O atoms were fully occupied (73 through 120 in our numbering as shown in Figure 4). Figure 8 shows the density contour maps of orbitals with the highest and lowest energies of the valence band. The highest energy orbital (120) showed the p orbital lobes on the O atom, indicating that the orbital was purely composed of the O 2p orbital. The lowest part of the band (73) was also formed by the O 2p orbital, but the In 5s5p orbitals mix into to some degree. This mixing is rather common for metal oxide semiconductors including the d^{10} elements, and the mixing occurred in only a few orbitals with the lowest energy. Thus, the valence band was composed of purely the O2p AOs except for a few orbitals in the lowest level. In a previous study of $ZnGa_2O_4$,[22] the DFT calculation showed covalent bond character between Zn and O atom and the upward shift of the valence band due to the O 2p−Zn 3d orbital repulsion. On the other hand, in $SrIn_2O_4$, there were no bonding interactions between Sr 4p−O 2p and In 4d−O 2p, since the In 4d orbital was located at deep core levels far from the O 2p orbital region.

Figure 9 shows the density contour maps of the lowest orbital as well as a little higher level's orbitals in the conduction band. The orbital 121 is the bottom of conduction band (LUMO), which is characterized by large dispersion in k-space. This orbital, shown in Figure 9a, is formed by the In 5s5p AOs with small mixing of the O 2p AO. This mixing is out of phase with the In5s5p AOs, in contrast with the "in phase" mixing shown in Figure 8b. Figure 9b shows the orbital locating at a little higher energy (129). From the nonspherical shape, significant contribution from the Sr 5s and also 4d AOs was apparent in this and higher orbitals.

The energy band diagram shows that the electron transfer upon illumination occurs from the O 2p orbital to the hybridized orbitals of In 5s and 5p. The large overlap among the In 5s and 5p AOs leads to large dispersion of the LUMO and hence the excited electrons in the conduction band have large mobility, which is related to better photocatalytic performance. In a previous study,[2] the band structures of $LiInO_2$ and $NaInO_2$ were

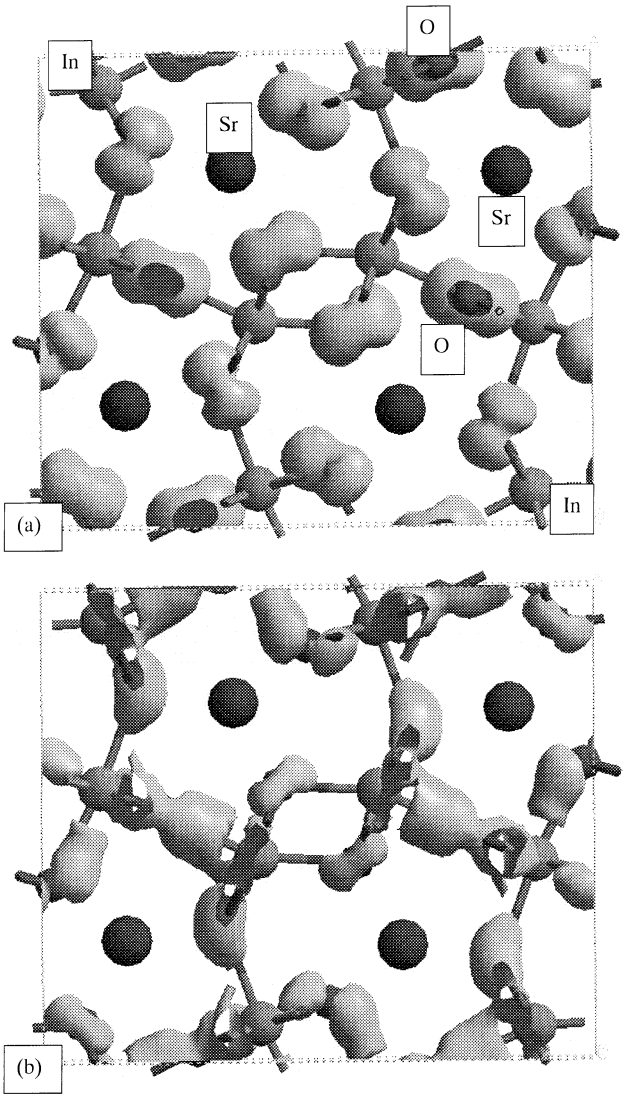

Figure 8. Density contour maps of orbitals at the top and bottom of the valence band for $SrIn_2O_4$: (a) orbital 120 with the highest energy (HOMO) and (b) orbital 73 with the lowest energy within the valence band.

calculated. The valence bands consisted of the O 2p orbitals, and the bottom of the conduction bands were composed of the In 5s and 5p orbitals. The band structures of alkaline metal indates were similar to those of alkaline earth metal indates. However, there were differences in the degrees of mixing with the In orbitals between alkaline metal and alkaline earth metal orbitals. The energy difference between the top of valence band and Sr 5s AO was 5.5 eV, whereas differences between the top of valence and Li 2s and Na 3s were 7.2 and 10.0, respectively. Thus, a larger overlap of Sr 5s with In 5s5p AO was present, compared to the overlap of Li 2s and Na 3s. The smallest mixing for $NaInO_2$ was rather strange but might be ascribable to a little longer Na−In distance, 0.331 nm, than 0.305 nm for $LiInO_2$.

$BaTi_4O_9$ is a representative transition metal oxide with octahedrally coordinated d^0 configuration. The DFT calculation showed that the valence band consisted of 54 orbitals, which corresponded to the 54 O 2p AOs in total, since the unit cell was $(BaTi_4O_9)_2$. Figure 10 shows the density contour maps of the orbitals with the highest (112) and the lowest energy (59) in the valence band. Both the orbitals were purely composed of the O 2p AOs, except a very small fraction of the Ti 3d AOs was seen for the latter. Thus, the character of the valence band is the same between d^{10} and d^0 configurations. This is a natural

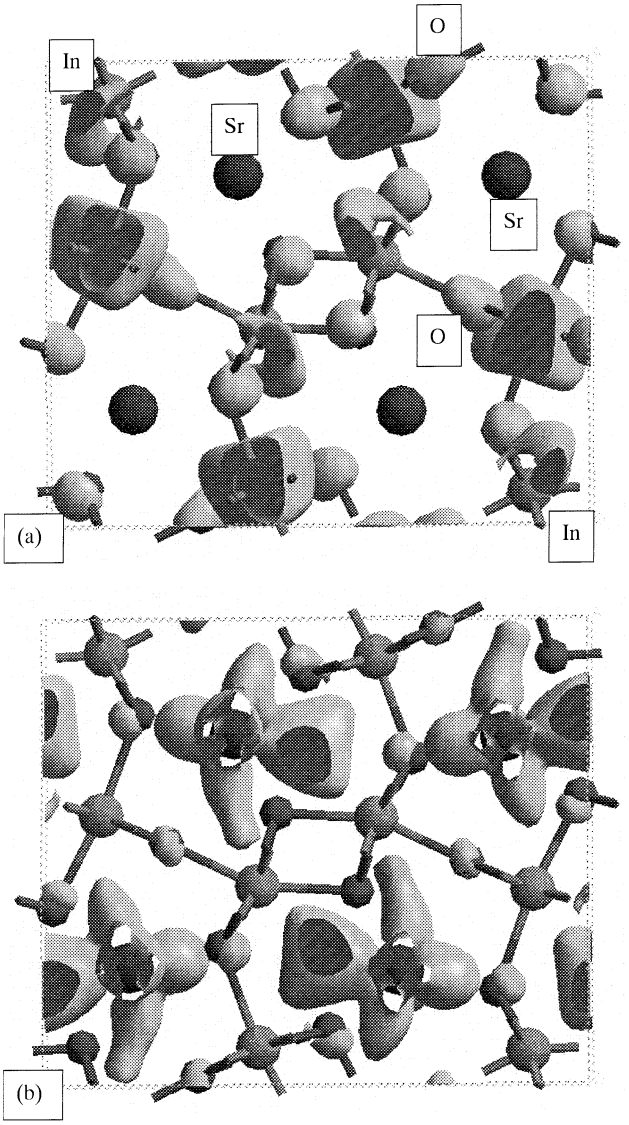

Figure 9. Density contour maps of orbitals at the lower part of the conduction band for $SrIn_2O_4$: (a) orbital 121 with the lowest energy (LUMO) and (b) orbital 129 with a little higher energy.

and common result for the metal oxide semiconductors unless some special elements such as Bi, Pb, or Ag are included. Figure 11 shows the density contour maps of orbitals with the lowest energy (113) and with a little higher energy (120) in the conduction band. Both the orbitals exclusively consisted of the Ti3d AOs. The mixing of Ti 3d AO with the O 2p AO was extremely small. Thus, the degree of hybridization in the valence and conduction bands was much smaller for $BaTi_4O_9$ than for $SrIn_2O_4$. Furthermore, the dispersion in k-space was quite small for the conduction band of $BaTi_4O_9$. There was an important difference in the conduction bands between $BaTi_4O_9$ and $SrIn_2O_4$, and thus it is evident that the characteristic feature of $SrIn_2O_4$ is broad s and p orbitals with large dispersion in the conduction band, which gives rise to a large mobility of photoexcited electrons.

Based on the above-mentioned findings, the following model can be proposed for a mechanism of photocatalysis by the alkaline earth metal indates with d^{10} configuration. The internal fields due to the dipole moment of distorted InO_6 octahedra promote the charge separation in the very initial process of photoexcitation, and diffused broad hybridized In 5s5p orbitals with large dispersion are useful for photoexcited electron transfers without recombination, which permits the photoexcited

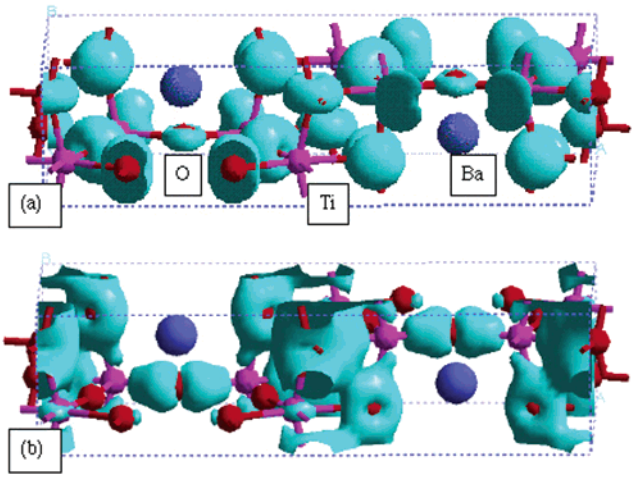

Figure 10. Density contour maps of orbitals at the top and bottom of the valence band for $BaTi_4O_9$: (a) orbital 112 with the highest energy (HOMO) and (b) orbital 59 with the lowest energy within the valence band.

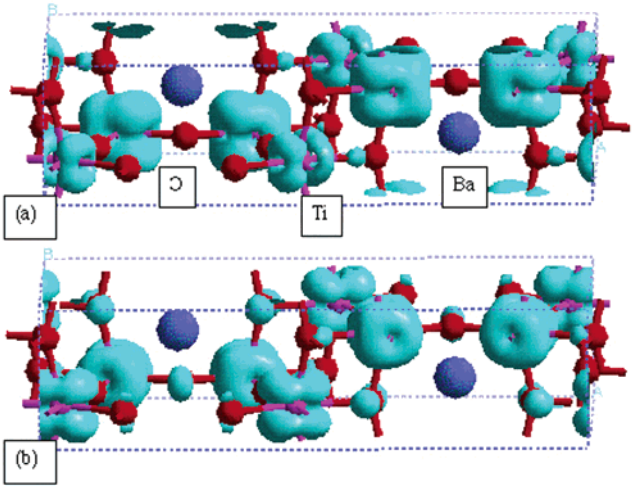

Figure 11. Density contour maps of orbitals at the lower part of the conduction band for $BaTi_4O_9$: (a) orbital 113 with the lowest energy (LUMO) and (b) orbital 120 with a little higher energy.

electrons to move to fine RuO_2 particles dispersed on the tunnel structure space. The p-block metal oxides with d^{10} configuration were evidently different in the conduction bands from transition metal oxides that had an octahedrally coordinated d^0 metal ion. This model predicts that almost all alkaline earth metal p-block metal oxides with large distortion of octahedral and tetrahedral units make good photocatalysts for water decomposition in combination with RuO_2.

Acknowledgment. The work was supported by CREST of JST and by Grant-in-Aid of Scientific Research of Priority Area (15033229) from the Ministry of Education, Science, and Culture.

References and Notes

(1) Sato, J.; Saito, S.; Nishiyama, H.; Inoue, Y. *J. Phys. Chem. B* **2003**, *107*, 7965 (preceding paper in this issue).

(2) Sato, J.; Kobayashi, H.; Saito, S.; Nishiyama, H.; Inoue, Y. *J. Photochem. Photobiol. A: Chem.* (in press).

(3) Von Schenck, R.; Mueller-Buschbaum, H. *Z. Anorg. Allg. Chem.* **1973**, *398*, 24.

(4) Lukaszewicz, K. *Roez. Chem.* **1957**, *31*, 1111.

(5) Templeton, D. H.; Dauben, C. H. *J. Chem. Phys.* **1960**, *32*, 1515.

(6) Hofmeister, W.; Tillmanns, E.; Baur, W. H. *Acta Crystallogr*. **1984**, *C 40*, 1510.
(7) Payne, M. C.; Teter, M. P.; Allan, D. C.; Arias, T. A.; Joannopoulos, J. D. *Rev. Mod. Phys*. **1992**, *64*, 1045.
(8) Vanderbilt, D. *Phys. Rev.* **1990**, *B41*, 7892.
(9) Criuckshank, F. R.; Taylor, D. MaK.; Glasser, F. P. *J. Inorg. Nucl. Chem*. **1964**, *26*, 937.
(10) Lalla, A.; Mueller-Buschbaum, H. *Z. Anorg. Allg. Chem*. **1990**, *588*, 117.
(11) Padurow; Schlusterius *Ber. Dtsch. Keram. Ges.* **1955**, *32*, 292.
(12) Hubbert-Paletta, E.; Hoppe, R.; Kreuzburg, G. *Z. Anorg. Allg. Chem*. **1970**, *379*, 255.
(13) Glaum, H.; Voigt, S.; Hoppe, R. *Z. Anorg. Allg. Chem*. **1991**, *598*, 129.
(14) Reid, A. F. *Inorg. Chem*. **1967**, *6*, 631.
(15) Sato, J.; Saito, S.; Nishiyama, H.; Inoue, Y. *J. Photochem. Photobiol. A: Chem.* **2002**, *148*, 85.
(16) Unpublished data.
(17) Inoue, Y.; Asai, Y.; Sato, K. *J. Chem. Soc., Faraday Trans*. **1994**, *90*, 797.
(18) Kohno, M.; Ogura, S.; Sato, K.; Inoue, Y. *Chem. Phys. Lett*. **1997**, *267*, 72.
(19) Inoue, Y.; Kubokawa, T.; Sato, K. *J. Phys. Chem*. **1991**, *95*, 4059.
(20) Ogura, S.; Kohno, M.; Sato, K.; Inoue, Y. *Phys. Chem. Chem. Phys*. **1999**, *1*, 179.
(21) Andersson, S.; Wadsley, A. D. *Acta Crystallogr*. **1962**, *15*, 194.
(22) Ikarashi, K.; Sato, J.; Kobayashi, H.; Saito, S.; Nishiyama, H.; Inoue, Y. *J. Phys. Chem.* **2002**, *106*, 9048.